Enhanced adsorption of sulfonated lignite with hierarchical porous-structure of MgAl-layered double hydroxide

Bingbing Bai[a], Chenye Yang[a], Chen Huang[b], Tao Yu[a,b], Gang Chen[a,c,*], Ying Tang[a,b,*]

[a]State Key Laboratory of Petroleum Pollution Control, Xi'an Shiyou University, 18# 2nd Dianzi Road, Xi'an 710065, China,
Tel.: +86-029-88382693; email: gangchen@xsyu.edu.cn (G. Chen)
[b]Shaanxi Province Key Laboratory of Environmental Pollution Control and Reservoir Protection Technology of Oilfields,
Xi'an Shiyou University, Xi'an 710065, China
[c]Engineering Research Center of Oil and Gas Field Chemistry, Universities of Shaanxi Provence, Xi'an Shiyou University,
Xi'an 710065, China

ABSTRACT

Sulfonated lignite (SL) is extensively utilized in petroleum exploration; however, its effective removal from wastewater poses a significant challenge. China's environmental protection department has classified it as a regulated oilfield chemical. In this study, hierarchically porous layered double hydroxide nanoparticles was prepared based on the soft template of cetyltrimethylammonium chloride and salicylic acid under hydrothermal condition. The effects of surfactant concentrations on the physical properties of the obtained adsorbents have been investigated by using X-ray powder diffraction, scanning electron microscopy, Brunauer–Emmett–Teller, and Fourier-transform infrared spectroscopy characterizations. It was found that three-dimensionally hydrotalcite nanosheets attached uniformly on the surface of soft template, generating higher crystallization and large specific area. Furthermore, the adsorption capacity of the material to SL was investigated to evaluate its application for the treatment of oilfield wastewater. The maximum adsorption capacity was equal to 854.70 mg/g at 298 K and pH of 7, which is significantly higher than the adsorption capacity of ordinary hydrotalcite (56.3 mg/g). The adsorption reaction followed the pseudo-second-order kinetics as well as the Freundlich isotherm model. Moreover, thermodynamic investigations showed that adsorption exhibits exothermic characteristics. After three adsorption–desorption cycles, hierarchically porous hydrotalcite nanoparticles still exhibit a high adsorption capacity of up to 187.7 mg/g. Anion exchange and electrostatic attraction were considered as the main adsorption mechanisms.

Keywords: Hierarchically porous hydrotalcite; Soft template; Sulfonated lignite; Adsorption; Wastewater

1. Introduction

Million tons of high-concentration toxic organic drilling wastewater is produced during the oilfield exploration in China every year [1–3]. Therefore, considering environmental and health reasons, how to effectively degrade drilling wastewater has always been a huge challenge and paid considerable attention. Sulfonated lignite (SL) is a widely used viscosity reducer, fluid loss reducer and pressure-reducing agent in the process of petroleum exploration [4–6]. However, high levels of the SL could pose a serious threat to human beings and ecological environment due to their unfavorable color and difficult degradability, which has been listed as a restricted oilfield chemical by China's environmental protection department. Up to now, various technologies have been developed to remove SL from oilfield wastewater, including chemical oxidation, membrane filtration, biological method, adsorption and so on [7–10].

* Corresponding author.

Among them, adsorption method has been recognized as the most alternative and promising technologies owning to its easy operation, strong flexibility, high efficiency and no secondary pollution [11]. However, most adsorbents may agglomerate together and are easily lost its activity during the adsorption process due to poor pore properties.

Layered double hydroxide (LDH), a class of two-dimensional nanostructured clay minerals, is composed of positively charged metal hydroxide layer together with crystalline water and charge-balancing anions in interlayer regions [12–14]. Due to its high surface areas, pore volumes, and adjustable pore sizes, LDHs exhibit potential advantage in the field of adsorption applications. However, the traditional hydrotalcite has a small interlayer spacing so as to be applied to the removal of small-molecule pollutants. To increase the adsorption capacity of macromolecular pollutants, surfactant has been used as soft template to obtain hierarchical LDHs materials with large number of active sites and specific morphologies [15]. Sun et al. [16] employed sodium citrate as a template combined with hydrothermal method to prepare 3D NiAl-LDH with a high specific surface area and hierarchical microstructure. The results demonstrated that the increased specific surface area facilitated the diffusion and desorption of pollutant molecules, leading to a significant enhancement in the removal efficiency of the adsorbent for nitrophenols.

Considering the urgency of treating sulfonated lignite and the superior structure of hydrotalcite prepared by the soft template method, this study aimed to synthesize a novel hierarchical hydrotalcite material with larger specific surface area, more abundant pore structure, and better morphology by employing cetyltrimethylammonium chloride (CTAC) and salicylic acid (SA) as soft templates via a hydrothermal approach. The material was subsequently employed as an adsorbent with the objective of achieving effective elimination of persistent organic pollutants, specifically sulfonated lignite found in oilfields.

2. Materials and methods

2.1. Materials

All chemicals including cetyltrimethylammonium chloride (CTAC), salicylic acid (SA), $Mg(NO_3)_2 \cdot 6H_2O$, $Al(NO_3)_3 \cdot 9H_2O$, urea, sodium hydroxide (NaOH) and absolute ethanol were analytical grade without any further purification, supplied by Xi'an Chemical Reagent Factory. Sulfonated lignite was purchased from Tarim, Xinjiang, China. Distilled water was used throughout the experiments.

2.2. Preparation of MgAl-LDH nanoparticles

A soft-template method was employed for the preparation of hierarchical MgAl-LDH under hydrothermal synthesis conditions [17]. Firstly, 3.04 g CTAC and 0.96 g SA were dispersed into 200 mL distilled water to get a surfactant solution with a mass concentration of 2.0%, which was considered as solution A. Then, 0.06 mol of $Mg(NO_3)_2$, 0.03 mol of $Al(NO_3)_3$ and 0.27 mol of urea was dissolved in 100 mL distilled water, which was considered as solution B. Solution B was slowly dropped into solution A under constant stirring until complete mixing of the solution. The

formed suspension was transferred to an autoclave aging at 160°C for 6 h [18]. After the aging step, the precipitate obtained was separated by centrifugation, washed extensively with distilled water until the pH of 7, subsequently dried at 80°C overnight. The resulting sample was labelled as 2% CS-LDH indicating the addition of CTAC and SA. To better understand and explore the best adsorption capacity of MgAl-LDH, surfactant concentrations of 1%, 2%, and 3% were investigated, and the obtained LDHs were designated as 1% CS-LDH, 2% CS-LDH, and 3% CS-LDH, respectively. For comparison, the traditional MgAl-LDH in the absence of surfactant solution was prepared and designated as LDH.

2.3. Characterization of materials

N_2 physisorption using ASAP 2020 equipment (Norcross, Georgia, USA) was applied to analyze the surface area and pore property of the materials. Morphologies of the obtained materials were characterized by scanning electron microscopy (JSM-6390A, Japan) with the applied voltage of 20 kV. The crystalline structure of as-prepared materials was analyzed by power X-ray diffraction device (XRD, JDX-3530, Japan) with Cu Kα radiation and a scanning speed of 2°/min at 40 kV voltage and 40 mA current. All infrared measurements were performed on a Nicolet 5700 Fourier-transform infrared spectrometer (FTIR, Thermo Electron Co., USA) in the range of 4,000–500 cm^{-1}.

2.4. Adsorption experiments

Adsorption processes for single factor experiments were carried out by adding 0.8 g/L adsorbent to 100 mg/L sulfonated lignite solutions with an initial pH value of 7 under stirred vigorously at room temperature for a given time. Then the residual concentration of sulfonated lignite was measured by UV-Vis spectrophotometry at the wavelength maximum absorbance of 300 nm. Adsorption kinetics study was conducted by adding 50 mg adsorbent into 100 mL of 100, 200 and 300 mg/L sulfonated lignite solutions. The adsorption isotherm was established by using different initial sulfonated lignite concentrations (100–500 mg/L) with an adsorbent dosage of 0.8 g/L. The initial solution pH in both studies was adjusted to be 7.0. Adsorption thermodynamic analysis was performed by adding 0.8 g/L adsorbent to 200 mg/L sulfonated lignite solution at 288, 298 and 308 K. The adsorption capacity (q_t) at any given time and at equilibrium was calculated according to Eq. (1):

$$q_t = \frac{(C_0 - C_e)}{m} \tag{1}$$

where C_0 (mg/L) and C_e (mg/L) was the initial and equilibrium concentration (mg/L) of sulfonated lignite, respectively, V (L) is the volume of solution and m (g) is the mass of the adsorbent.

3. Results and discussion

3.1. Structural characterization of MgAl-LDH nanoparticles

Fig. 1 presents the XRD spectra of hydrotalcite samples prepared under different surfactant concentrations.

According to the standard reference (PDF#54-1030), the hydrotalcite sample synthesized via the hydrothermal method without a soft template exhibited characteristic crystal planes (003), (006), (012), (015), (018), (110), and (113) of LDH materials at $2\theta = 11.2°, 22.9°, 34.3°, 38.9°, 46.4°, 60.4°$ and $61.8°$ [19]. When the surfactant micelles were added, the characteristic peaks of hydrotalcite still remained indicating the layered structure of MgAl-LDH. However, it was observed that the intensity of the diffraction peaks in different concentrations of surfactant solutions weakened with the increase of the surfactant concentration, which should be due to that the high viscosity in high concentration of micelles solution affects the crystallization of hydrotalcite.

Table 1 shows the pore structure parameters of ordinary hydrotalcite (LDH) and the prepared hydrotalcite in different concentrations of surfactants solutions. The corresponding nitrogen adsorption and desorption curves, as well as the pore size distribution curve, are shown in Fig. 2. It can
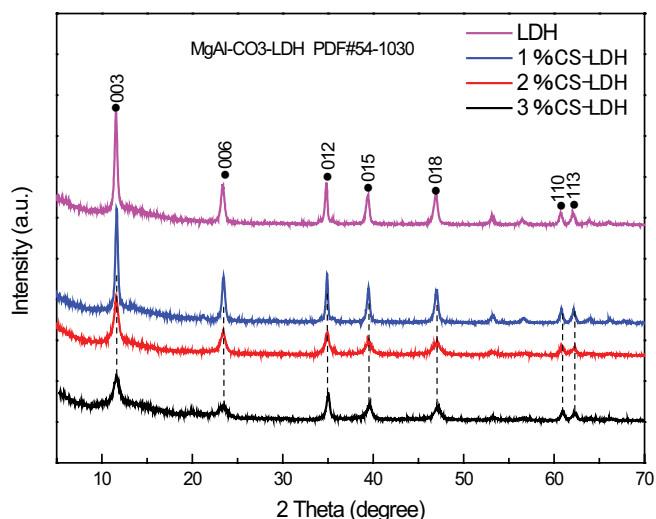
be seen from Table 1 that the specific surface area, pore volume, and average pore diameter of ordinary hydrotalcite are only 44.5212 m²/g, 0.2039 cm³/g, and 15.7091 nm, respectively. However, the introduction of surfactant colloidal templates led to a distinct increase of prepared hydrotalcite in porous structure. When the total concentration of surfactant is 2% and concentration of metal salt solution is 0.9 mol/L, the specific surface area and pore volume of prepared 2% CS-LDH reach 197.9862 m²/g and 0.5003 cm³/g, respectively, which are higher than the ordinary hydrotalcite, indicating the rich pore structure in the newly prepared hydrotalcite. Fig. 2a illustrates that the N_2 adsorption–desorption isotherms of the four samples exhibited a type IV isotherm, thus indicating the existence of mesopores. However, an apparent hysteresis loop could be distinguished on the adsorption–desorption isotherms of 2% CS-LDH reflecting the increase of the adsorption capacity at higher relative pressure due to the existence of macropores [20]. This result can be seen from the broad size distribution of the hydrotalcite (2% CS-LDH) from 5 to 50 nm in Fig. 2b, revealing the excellent adsorption performance of the prepared 2% CS-LDH.

In order to understand the role of surfactant micelle template, the field-emission scanning electron microscopy was applied to analyze the morphology of the as-obtained ordinary hydrotalcite (LDH) and prepared hydrotalcite (2% CS-LDH). It can be seen from Fig. 3a that ordinary hydrotalcite (LDH) shows a regular lamellar structure with an average diameter of 2–3 μm, and there is overlap between the layer and the layer.

Fig. 1. X-ray diffraction patterns of hydrotalcite prepared in surfactants solutions of different concentrations by hydrothermal method (*a* = 0, *b* = 1%, *c* = 2%, *d* = 3%).

Table 1
Pore structure parameter of prepared hydrotalcite

Sample	Specific area (m²/g)	Pore volume (cm³/g)	Pore diameter (nm)
LDH	44.5212	0.2039	15.7091
1% CS-LDH	64.2220	0.3163	19.6984
2% CS-LDH	197.9862	0.5003	10.1082
3% CS-LDH	51.9103	0.2446	21.9747
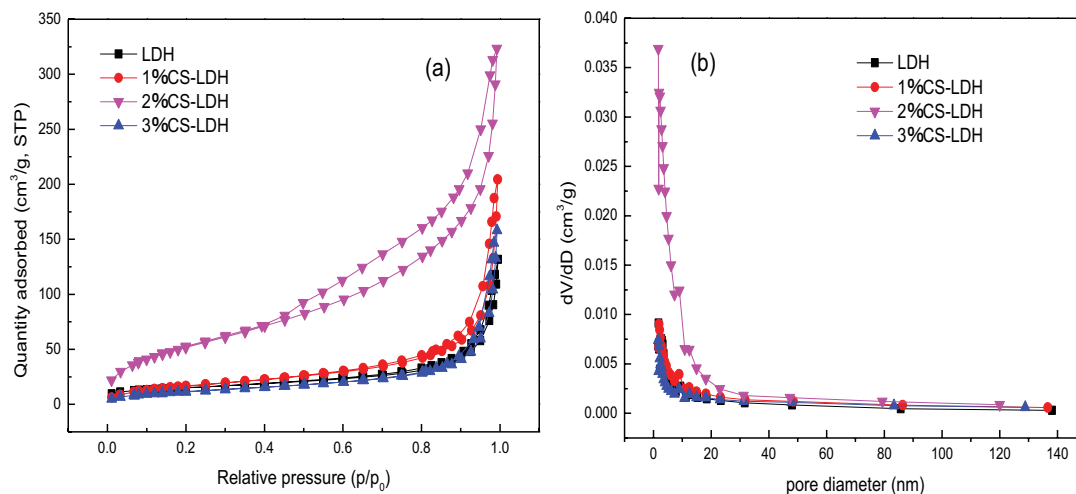
Fig. 2. Nitrogen adsorption–desorption isotherms (a) and corresponding pore-size distribution curve (b) of prepared hydrotalcite.

However, when 2% surfactant micelles were added, Fig. 3b shows the morphology of the material changes significantly and the plate layer cross-aggregated with each other, forming a more regular and orderly staggered structure, which would greatly increase the specific surface area of the material so as to provide more active adsorption site.

Fig. 4 presents the FTIR spectrum of ordinary hydrotalcite (LDH) and prepared hydrotalcite (2% CS-LDH) aged at 160°C for 6 h. For the two types of hydrotalcite, the remarkable peaks at 3,448–3,453 cm^{-1} and 1,601–1,635 cm^{-1} are assigned to the stretching vibrations of the hydroxyl groups in the hydrotalcite layer and the interlayer water molecules [17]. Another adsorption band around 1,384 cm^{-1} corresponded to the asymmetric stretching vibration of C–O, indicating the existence of CO_3^{2-} on the hydrotalcite [21]. The peaks in the range of 900–400 cm^{-1} are attributed to metal-oxygen stretching, metal-hydroxyl stretching, and deformation vibration modes of metal-oxygen in hydrotalcite layers. However, it was found that the two new characteristic bands of 2% CS-LDH at 2,850 and 2,919 cm^{-1} related to the CH_2 bending vibration, indicating the combination between the surfactant and the hydrotalcite surface [22].

The formation process of the hierarchical MgAl-LDH based on the above analysis is shown in Fig. 5. In the stable three-dimensional network structure composed of CTAC and SA, the positive charge (CTAC$^+$) of the CTAC molecule and the oxygen anion of the salicylate ion (Sal$^-$) attract each other, causing a lot of chloride anions (Cl$^-$) to be released into the solution (Fig. 5a). After the mixed metal salt solution was added, urea gradually decomposes with the increase of temperature and the hydroxyl product of metals was formed. Since the solubility product constant of $Al(OH)_3$ is much smaller than that of $Mg(OH)_2$, Al^{3+} preferentially formed a large amount of hydrotalcite precursors ($Al(OH)_4^-$). When the precipitation conditions of Mg^{2+} reaches, it begins to precipitate and produces a large number of hydrotalcite nuclei, which then grow into hydrotalcite nanosheets (Fig. 5b). Due to a large number of positive charges on the hydrotalcite layer, it will attract the free Cl$^-$ in the solution under the action of electrostatic gravity (Fig. 5c), and the resulting hydrotalcite nanosheets will grow staggered along the micellar interface (Fig. 5d).

3.2. Adsorption performance

3.2.1. Effect of different adsorbents

Sulfonated lignite was chosen as the target contaminant to study the adsorption behavior of as-prepared hydrotalcite derived from micellar template. As shown in Fig. 6a, under the conditions of 25°C, the initial pH of the solution 7, the amount of adsorbent 0.08 g, and the initial sulfonated lignite concentration of 100 mg/L, the removal effect of hydrotalcite containing micellar template had significantly better removal efficiency for sulfonated lignite. With increasing the surfactant concentrations from 0% to 2% the adsorption capacity increased from 56.3 to 115.5 mg/g with the removal rate from 45.0% to 92.4%, respectively. In combination with the morphology of 2% CS-LDH, it may be related to the large specific surface area exposed more active adsorption sites, thereby enhancing the removal effects. However, the adsorption capacity and removal rate decreased to 111.5 mg/g and 89.2% when the surfactant concentration increase to
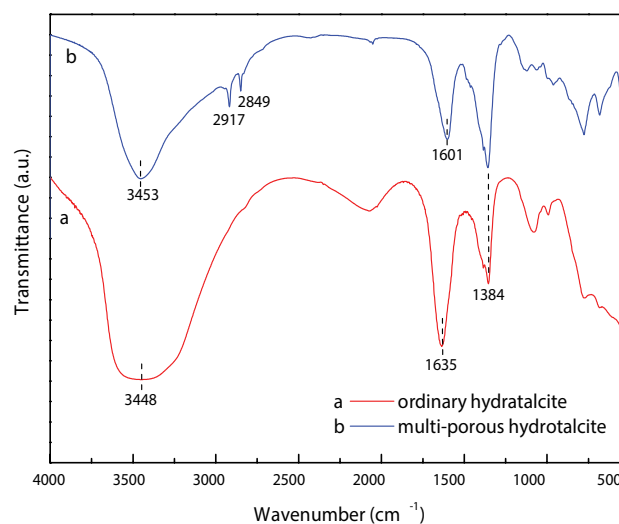
Fig. 4. Fourier-transform infrared spectra of hydrotalcite (a) ordinary hydrotalcite and (b) hierarchical hydrotalcite.

Fig. 3. Scanning electron microscopy images of ordinary hydrotalcite (a) and hierarchical MgAl-LDH (b).
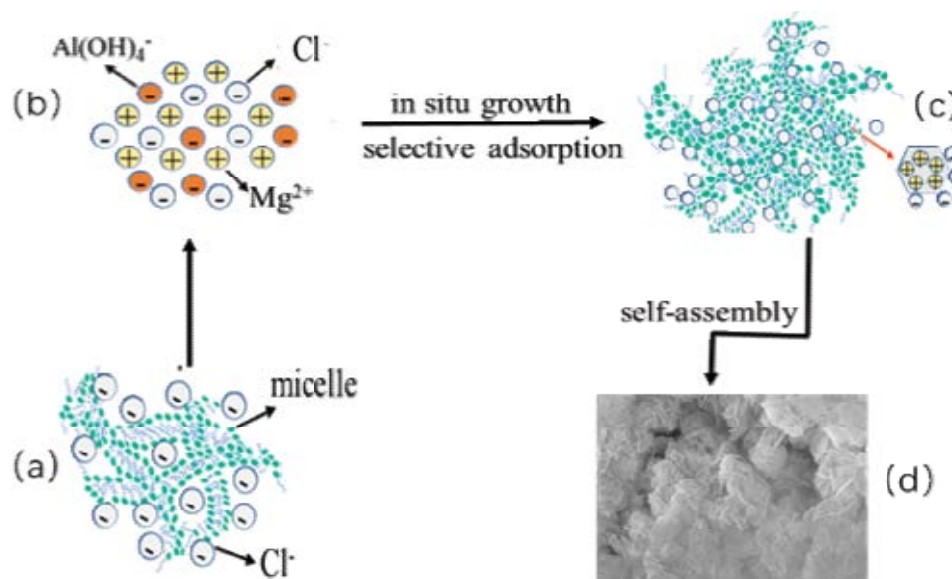
Fig. 5. The construction process of hierarchical hydrotalcite (a) represents the aggregation of surfactant micelles, (b) represents adsorption and dispersion of the metal salt solution and surfactant micelles, (c) represents the interaction between the hydrotalcite and surfactant micelle, and (d) represents the surface morphology of hierarchical hydrotalcite nanoparticles.

3% due to the incomplete mixing of the high-viscosity surfactant and the metal salt solution. Therefore, 2% CS-LDH was used as the adsorbent in subsequent experiments.

3.2.2. Effect of absorbent dosage

The adsorbent dosage plays a role in the removal performance of pollutant [23]. The effects of the amount of adsorbent varied from 0.2 to 1.2 g/L were investigated at an initial SL concentration of 100 mg/L, 25°C and pH of 7. As the results shown in Fig. 6b, it can be found that as the adsorbent dose increased from 0.2 to 0.6 g/L, the SL removal efficiency remarkably increased from 59.4% to 97.9% due to the increasing active sites on the surface of the adsorbent which are proportional to the amount of adsorbent within a certain range. When the amount of adsorbent exceeds 0.6 g/L, the adsorption capacity keeps decreasing continuously with unchanged the SL removal rate, which should be due to excessive adsorption sites for the sulfonated lignite molecules in the solution so as to the decrease of adsorption effects. Comprehensive consideration of the results of combined adsorption capacity and removal rate, 0.8 g/L was selected as the optimal dosage in the following experiments.

3.2.3. Effect of initial solution pH

At room temperature, the effect of solution pH on SL adsorption performance on 2% CS-LDH was evaluated at initial SL concentration of 200 mg/L and the adsorbent dosage of 0.8 g/L. It was observed from Fig. 6c that the adsorption capacity shows a decrease with an increasing pH from 4 to 13. The removal rate decreases from 99.8% to 93.1% with increasing the pH from 3 to 7 indicating the strong electrostatic attraction between SO_3^- in the sulfonated lignite and H^+ in the solution under acidic conditions [24].

The removal rate stabilized at 93.0% when the pH was set in range from 7 to 9. However, by further increasing the pH of the solution to 13, SL is partially ionized to SO_4^{2-}, so the removal rate of sulfonated lignite decreased to 88.7%.

3.2.4. Kinetic studies

To establish the mechanism, adsorption data were fitted by pseudo-first-order, pseudo-second-order, intraparticle diffusion models, and liquid film diffusion models [25]. The obtained adsorption kinetics and parameters calculated from the four adsorption equations are summarized in Fig. 7 and Table 2, respectively. The pseudo-second-order model exhibited higher correlation coefficient (R^2 is 1, 0.999, 0.998, respectively), while the fitting of pseudo-second-order model was found not to be satisfactory (R^2 is in the range of 0.794–0.926). Furthermore, as shown in Table 2, the experimental equilibrium capacity ($q_{e,exp}$) at different concentration is 121.80, 248.14, and 349.65 mg/g in the pseudo-second-order model, which is close to the calculated equilibrium capacity (122.54, 240.16, and 364.58 mg/g, respectively). Therefore, the rate-limiting step may be chemical adsorption involving valence forces through the ion exchange between 2% CS-LDH and SL. Meanwhile, the adsorption of SL is governed by either the intraparticle mass transport rate or the liquid phase mass transport rate. The experiment data of 2% CS-LDH fitted well to the intraparticle diffusion model with higher correlation coefficients (R^2 can reach up to 0.99), which indicates that the intraparticle diffusion model is the rate-controlling step [26].

3.2.5. Adsorption isotherm

Adsorption isotherms describe the interaction between the target pollutant and adsorbent [27], which were used to determine the maximum adsorption capacity of 2% CS-LDH
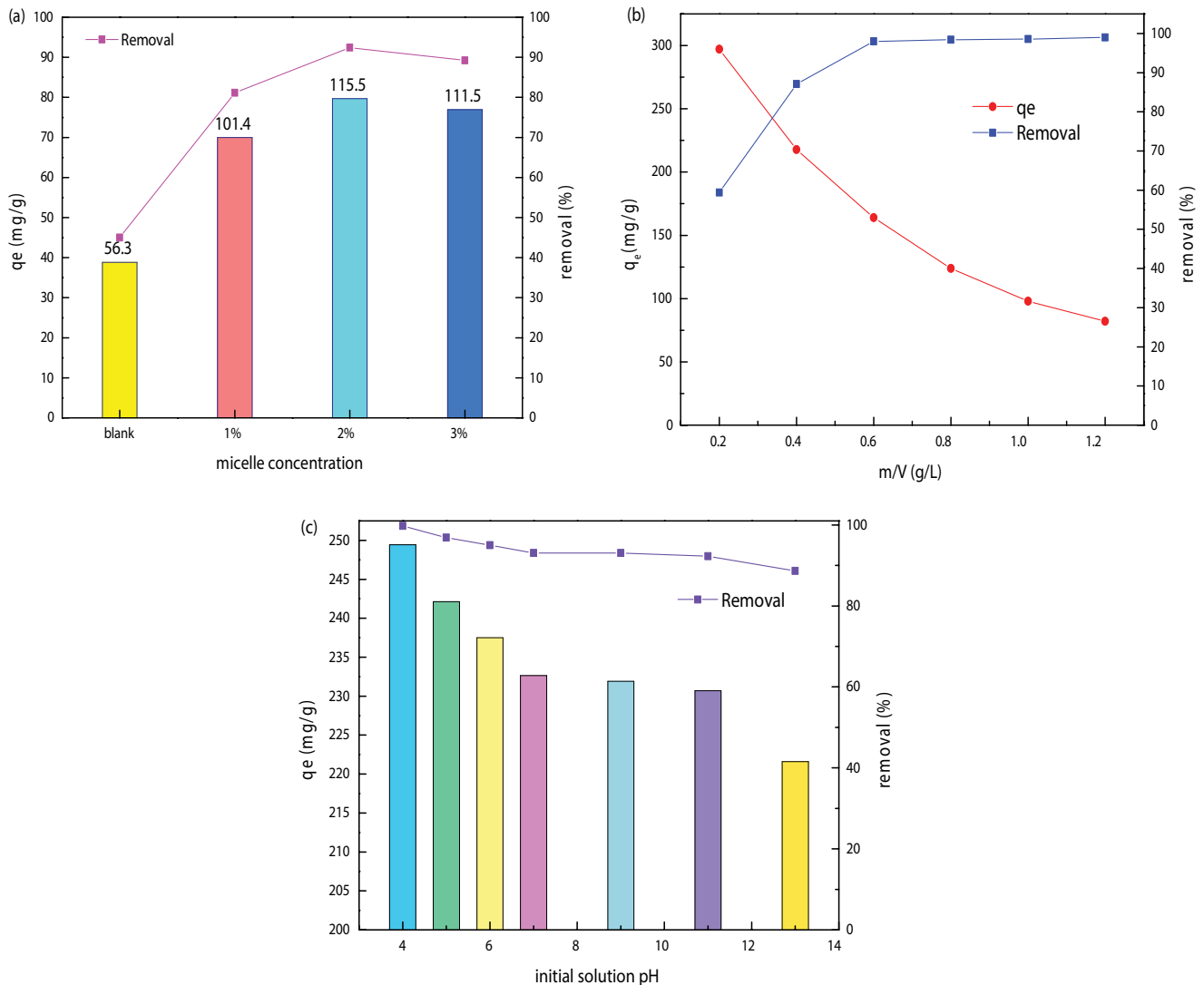
Fig. 6. (a) Effects of surfactant concentrations on SL adsorption, effects of adsorbent dosage (b) and solution pH (c) on SL adsorption using 2% CS-LDH (conditions: initial SL concentration of 100 mg/L, 25°C, pH = 7, and contact for 6 h).

to SL. The well-known Langmuir, Freundlich and Dubinin–Radushkevich model were used to describe the adsorption behavior of sulfonated lignite, and the corresponding fitting isotherms are shown in Fig. 8. According to the R^2 values presented in Table 3, the Freundlich model presented better values compared to Langmuir model, demonstrating that the formation of irregular multilayer adsorption on the surface of the adsorbent [28]. Moreover, all of the calculated n values are greater than 1 (1.6569 and 1.7365 at 298 and 303 K), proving that the adsorption process is favorable. It was observed from the Dubinin–Radushkevich model that the values of activation energy (E) are both less than 8 kJ/mol (366.3 and 395.1 J/mol at 298 and 303 K), indicating that the main adsorption force is electrostatic attraction [29].

3.2.6. Thermodynamic studies

Thorough assessment of thermodynamic parameters provides profound insights into the intrinsic energy changes associated with adsorption. In this study, the standard Gibbs free energy change ($\Delta G°$), the standard enthalpy change ($\Delta H°$) and the standard entropy change ($\Delta S°$) were evaluated by utilizing the adsorption isotherms in conjunction with Eqs. (2) and (3) [30].

$$\Delta G° = -RT \ln K \tag{2}$$

$$\ln K = \frac{\Delta S°}{R} - \frac{\Delta H°}{RT} \tag{3}$$

where K represents the equilibrium constant, R denotes the gas constant, and T signifies the temperature (K). The fitting isotherms are shown in Fig. 9, and the calculated thermodynamic parameters ($\Delta G°$, $\Delta H°$ and $\Delta S°$) are summarized in Table 4. It became more negative of $\Delta G°$ with decreases in temperature (−8.15, −7.70, and −7.15 kJ/mol at 288, 298, and 308 K, respectively), making the adsorption more favorable with the decrease in temperature [31]. The value of $\Delta H°$ is
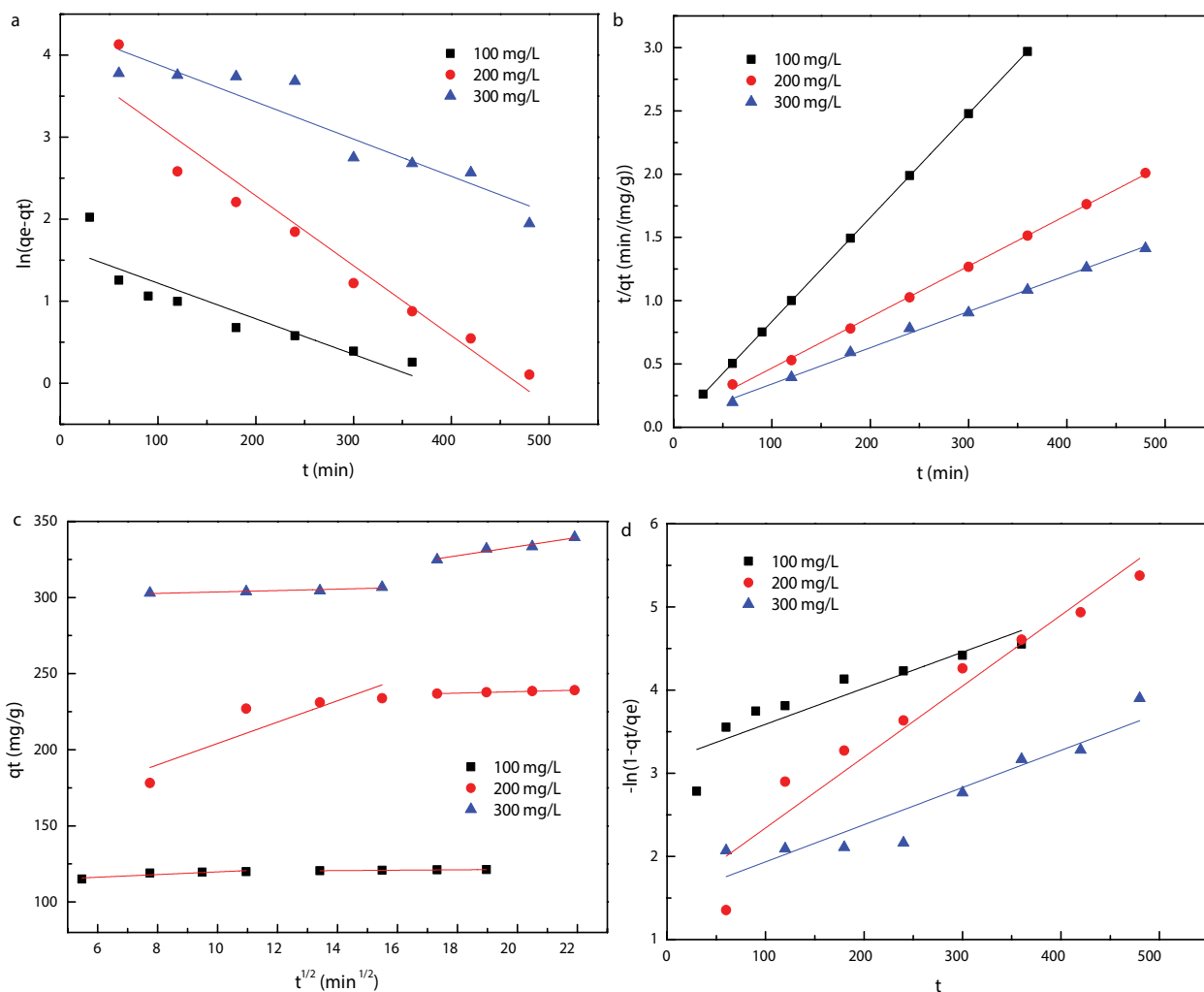
Fig. 7. Four kinetic models for the adsorption of SL by 2% CS-LDH: (a) pseudo-first-order, (b) pseudo-second-order, (c) particle internal diffusion, and (d) liquid film diffusion.

Table 2
Parameters of the four dynamics models

Models	Parameters	Concentration (mg/L)		
		100	200	300
Pseudo-first-order	$q_{e,cal}$ (mg/g)	5.22	54.14	76.43
	K_1 (h^{-1})	0.0043	0.0085	0.0045
	R^2	0.794	0.926	0.856
Pseudo-second-order	$q_{e,cal}$ (mg/g)	121.80	248.14	349.65
	$q_{e,exp}$ (mg/g)	122.54	240.16	364.58
	K_2 (g/m·gh)	0.0049	0.0003	0.0001
	R^2	1	0.999	0.998
Intraparticle diffusion	K_{i1} (mg/gh$^{1/2}$)	0.8767	7.0151	0.4663
	R_1^2	0.721	0.677	0.827
	K_{i2} (mg/gh$^{1/2}$)	0.1260	0.4923	3.0016
	R_2^2	0.978	0.990	0.931
Liquid film diffusion	K_{fd} (h^{-1})	0.0043	0.0085	0.0045
	R^2	0.824	0.926	0.869

negative indicating the exothermic nature. Simultaneously, the values of $\Delta S°$ also negative indicates the decrease in the degrees of freedom for the adsorption process [32,33].

3.3. Regeneration of adsorbent

Adsorption regeneration cycles were performed to investigate the durability of the adsorbent after long use. In the regeneration study, sodium hydroxide (NaOH) was used as eluents. At room temperature, 2% CS-LDH with saturated adsorption was immersed at pH of 13 under stirred for 12 h to achieve the desorption process. After the period of time, the sample was centrifuged, washed and dried at 60°C for 4 h for further use for the repeated evaluation. Subsequently, the regeneration test was investigated when the initial concentration of the SL is 200 mg/L at 25°C and pH of 7, and the results were shown in Fig. 10. After three cycles of regeneration, the adsorption capacity of 2% CS-LDH to sulfonated lignite slightly decreased from 235.4 to 187.7 mg/g, reflecting the decrease in adsorption performance of the prepared hierarchical hydrotalcite. As shown in Fig. 11, the
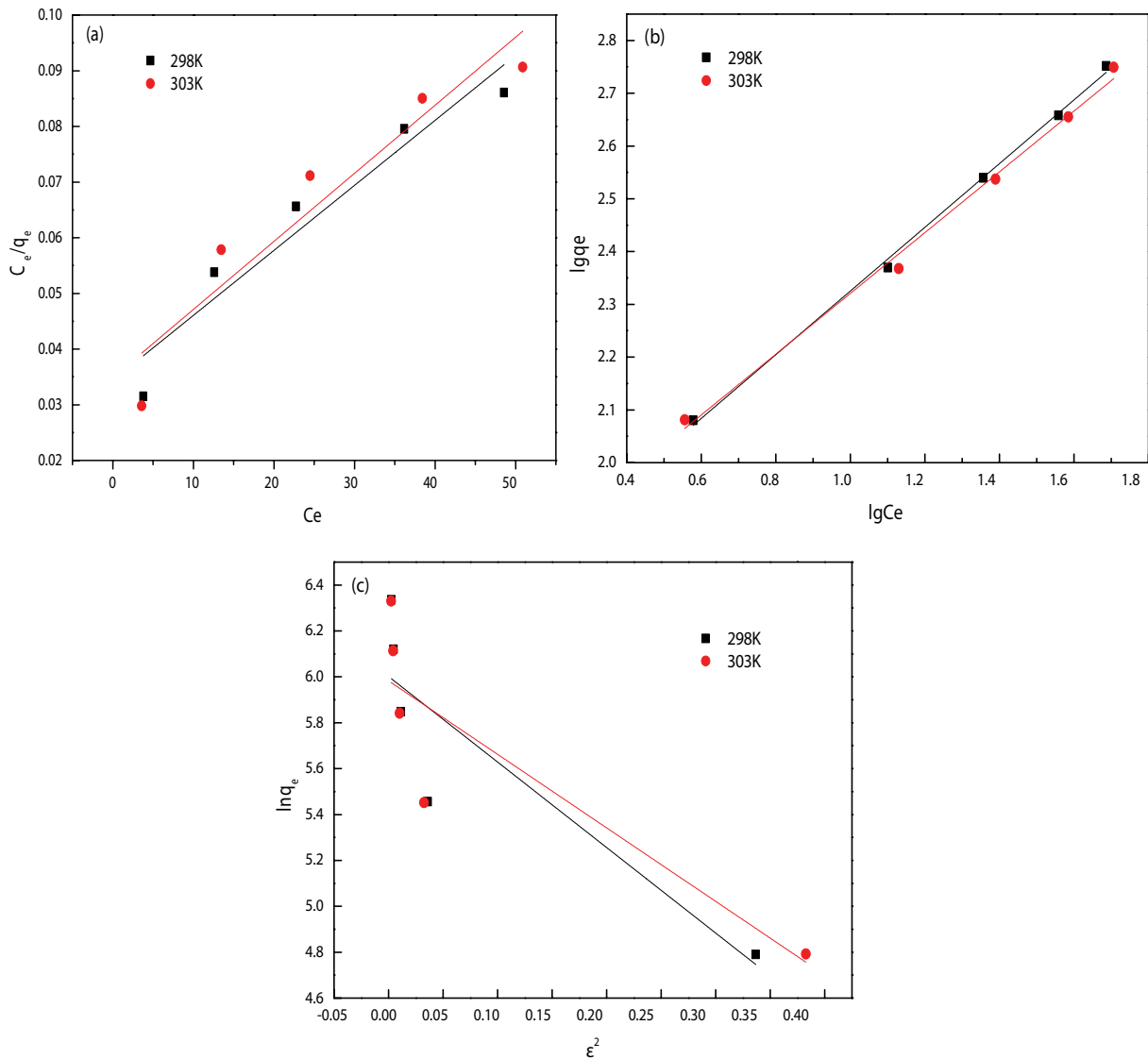
Fig. 8. Adsorption isothermal models for adsorption of SL by 2.8% CS-LDH: (a) Langmuir model, (b) Freundlich model, and (c) Dubinin–Radushkevich model.

Table 3
Isothermal model parameters of SL adsorption by 2.8% CS-LDH

Models	Parameters	Temperature	
		298 K	303 K
Langmuir	$q_{m,\text{cal}}$ (mg/g)	854.70	819.67
	K_L (L/mg)	0.0340	0.0350
	R^2	0.908	0.874
Freundlich	K_F (L/g)	52.6890	55.5699
	n	1.6569	1.7365
	R^2	0.998	0.996
Dubinin–Radushkevich model	q_m (mg/g)	403.97	396.47
	β (mol²/kJ²)	3.7264	3.2035
	R^2	0.714	0.690
	E (J/mol)	366.3	395.1

characteristic peaks of the hierarchical hydrotalcite at 22.9° (006) disappear, and the series of characteristic diffractions at 11.2° (003), 34.3° (012), 38.9° (015), 46.4° (018), 60.1° (110) and 61.5° (113) decreased in intensity after adsorption, which indicates that the layered structure of 2% CS-LDH was partially destroyed in adsorption reaction.

3.4. Adsorption mechanism of hierarchical hydrotalcite

In order to better discuss the adsorption mechanism, infrared spectrum analysis of the as-prepared 2% CS-LDH after adsorption was carried out (Fig. 12). By comparing the FTIR spectra of fresh 2% CS-LDH, the peak shift from 1,384 to 1,420 cm⁻¹ could be ascribed to the intercalation of $-SO_3^-$ in SL molecule [34]. Moreover, the symmetrical stretching vibration of O=S=O at 1,075 cm⁻¹ after adsorption is a clear evidence of the adsorption of SL onto 2% CS-LDH. Moreover, the shifting of stretching vibration bands of
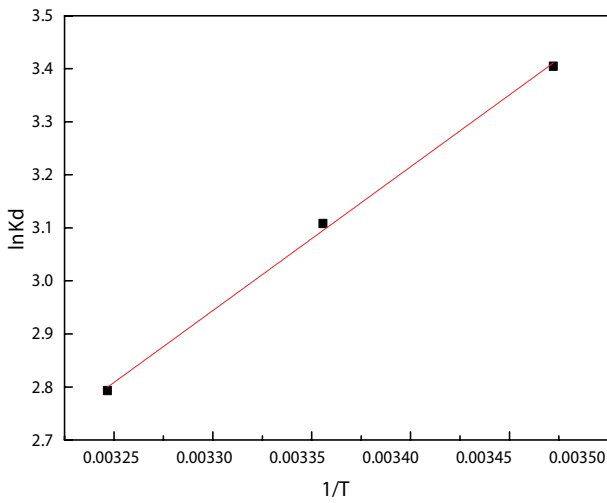
Fig. 9. Linear plot of $\ln K_d$ vs. $1/T$ for adsorption of SL by 2% CS-LDH at different temperature.

Table 4
Thermodynamic parameters for adsorption of SL by 2% CS-LDH

T (K)	$\Delta S°$ [J/(mol·K)]	$\Delta H°$ (kJ/mol)	$\Delta G°$ (kJ/mol)	R^2
288			−8.15	
298	−49.97	−2.25	−7.70	0.997
308			−7.15	
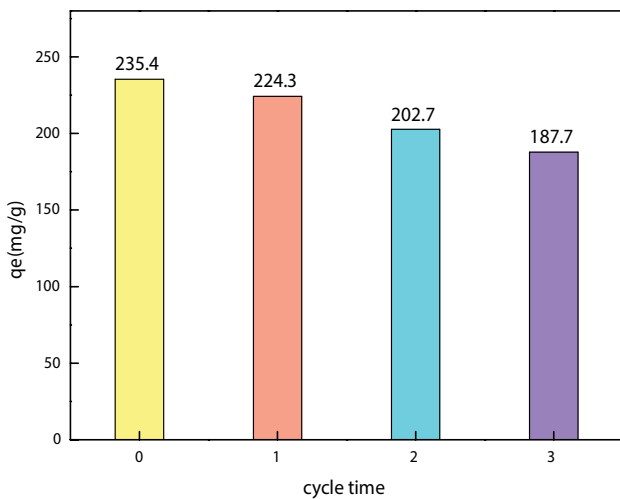
Fig. 10. Regeneration performance of SL by 2% CS-LDH.

O–H to a slight wavenumber from 3,451 to 3,448 cm⁻¹ indicating that the formation of coordination bonds between the SL molecule and hydrotalcite [35]. In conclusion, the adsorption of SL onto 2% CS-LDH could be speculated to occur through these steps (Fig. 13). Firstly, adsorption for SL occurred at the surface of the adsorbent through electrostatic attraction between the $-SO_3^-$ of SL and the positive charge on the hydrotalcite laminate (Fig. 13a). In addition,
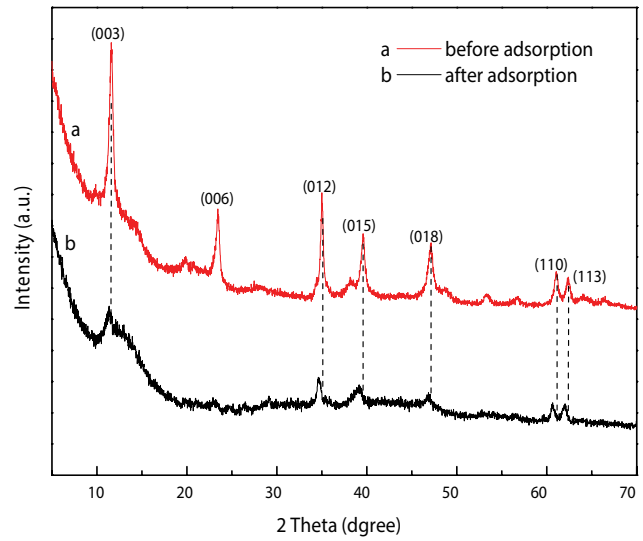
Fig. 11. X-ray diffraction patterns of 2% CS-LDH before and after adsorption.
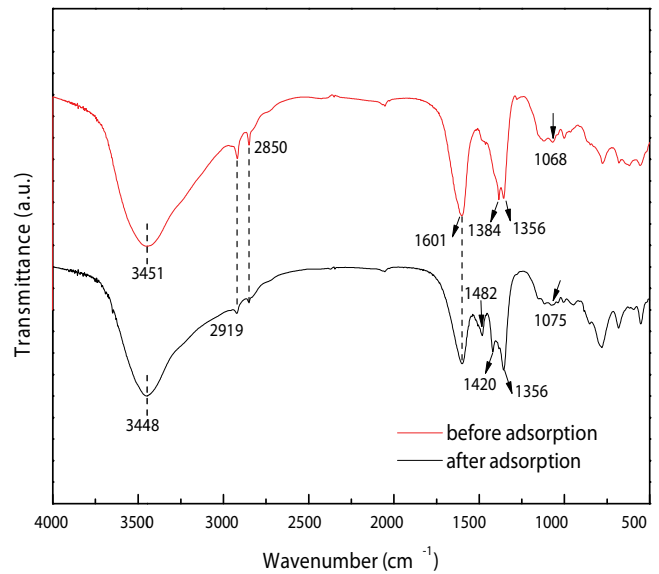
Fig. 12. Fourier-transform infrared spectra of 2% CS-LDH before and after adsorption.
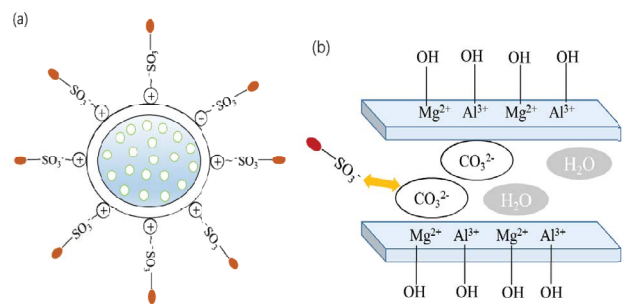
Fig. 13. Schematic illustration of SL adsorption by 2% CS-LDH.

the meso-macroporous networks of 2% CS-LDH provide more accessible diffusion pathways for adsorbates (Fig. 13a) and then, followed by anion exchange [36], the CO_3^{2-} in the interlayer of hydrotalcite is replaced by $-SO_3^-$ in the sulfonated lignite (Fig. 13b).

4. Conclusions

In this study, the hierarchical hydrotalcite with multistage pore structure was successfully prepared via hydrothermal synthesis approach, applying CTAC and SA as soft colloidal templates. It is worth noting that the specific surface area of the hydrotalcite with mesoporous and macroporous structure is as high as 197.9862 m^2/g which can effectively improve the adsorption performance. Kinetic and adsorption isotherm models show that the adsorption of sulfonated lignite on the hierarchical hydrotalcite follows the quasi-second-order kinetic model and Freundlich model. Meanwhile, thermodynamic data reveals that adsorption is an exothermic reaction. The main adsorption mechanism of the material is ion exchange and electrostatic attraction, and it is very suitable for adsorbing anionic pollutants in oilfields. This work will benefit the related research in oil field wastewater disposal.

Acknowledgement

References

[1] Y. Tang, L. Zhou, Y. Xue, X. Gu, J. Zhang, C. Qu, Preparation of nanoscale zero-valent metal for catalyzed clean oxidation of hydroxypropyl guar gum at a wide pH range, Desal. Water Treat., 197 (2020) 328–334.
[2] Y. Tang, L. Zhou, Z. Xu, J. Zhang, C. Qu, Z. Zhang, Heterogeneous degradation of oil field additives by Cu(II) complex-activated persulfate oxidation, Environ. Prog. Sustainable Energy, 40 (2021) e13562, doi: 10.1002/ep.13562.
[3] L. Zhou, Z. Xu, J. Zhang, Z. Zhang, Y. Tang, Degradation of hydroxypropyl guar gum at wide pH range by a heterogeneous Fenton-like process using bentonite-supported Cu(0), Water Sci. Technol., 82 (2020) 1635–1642.
[4] R. Zhang, B. Wang, H. Ma, Studies on chromium(VI) adsorption on sulfonated lignite, Desalination, 255 (2010) 61–66.
[5] M. Ilg, J. Plank, A novel kind of concrete superplasticizer based on lignite graft copolymers, Cem. Concr. Res., 79 (2016) 123–130.
[6] Y. Cui, F. Jiao, Q. Wei, X. Wang, L. Dong, Flotation separation of fluorite from calcite using sulfonated lignite as depressant, Sep. Purif. Technol., 242 (2020) 116698, doi: 10.1016/j.seppur.2020.116698.
[7] Y. Tang, Z. Li, Z. Xu, J. Zhang, C. Qu, Z. Zhang, Synthesis of hierarchical MgO based on a cotton template and its adsorption properties for efficient treatment of oilfield wastewater, RSC Adv., 10 (2020) 28695–28704.
[8] E. Lorenc-Grabowska, G. Gryglewicz, Adsorption of lignite-derived humic acids on coal-based mesoporous activated carbons, J. Colloid Interface Sci., 284 (2005) 416–423.

[9] M.S. Gasser, H.T. Mohsen, H.F. Aly, Humic acid adsorption onto Mg/Fe layered double hydroxide, Colloids Surf., A, 331 (2008) 195–201.
[10] C. An, S. Yang, G. Huang, S. Zhao, P. Zhang, Y. Yao, Removal of sulfonated humic acid from aqueous phase by modified coal fly ash waste: equilibrium and kinetic adsorption studies, Fuel, 165 (2016) 264–271.
[11] H. Chen, J. Lin, N. Zhang, L. Chen, S. Zhong, Y. Wang, W. Zhang, Q. Ling, Preparation of MgAl-EDTA-LDH based electrospun nanofiber membrane and its adsorption properties of copper(II) from wastewater, J. Hazard. Mater., 345 (2018) 1–9.
[12] A. Kheradmand, M. Negarestani, S. Kazemi, H. Shayesteh, S. Javanshir, H. Ghiasinejad, E. Jamshidi, Design and preparation magnetic bio-surfactant rhamnolipid-layered double hydroxide nanocomposite as an efficient and recyclable adsorbent for the removal of Rifampin from aqueous solution, Sep. Purif. Technol., 304 (2023) 122362, doi: 10.1016/j.seppur.2022.122362.
[13] X. Guo, P. Yin, H. Yang, Superb adsorption of organic dyes from aqueous solution on hierarchically porous composites constructed by ZnAl-LDH/Al(OH)$_3$ nanosheets, Microporous Mesoporous Mater., 259 (2018) 123–133.
[14] A. Kuznetsova, P.M. Domingues, T. Silva, A. Almeida, M.L. Zheludkevich, J. Tedim, M.G.S. Ferreira, A. Cunha, Antimicrobial activity of 2-mercaptobenzothiazole released from environmentally friendly nanostructured layered double hydroxides, J. Appl. Microbiol., 122 (2017) 1207–1218.
[15] J. Zhang, X. Xie, C. Li, H. Wang, L. Wang, The role of soft colloidal templates in the shape evolution of flower-like MgAl-LDH hierarchical microstructures, RSC Adv., 5 (2015) 29757–29765.
[16] Y. Sun, J. Zhou, W. Cai, R. Zhao, J. Yuan, Hierarchically porous NiAl-LDH nanoparticles as highly efficient adsorbent for p-nitrophenol from water, Appl. Surf. Sci., 349 (2015) 897–903.
[17] X.-Y. Yu, T. Luo, Y. Jia, R.-X. Xu, C. Gao, Y.-X. Zhang, J.-H. Liu, X.-J. Huang, Three-dimensional hierarchical flower-like Mg–Al-layered double hydroxides: highly efficient adsorbents for As(V) and Cr(VI) removal, Nanoscale, 4 (2012) 3466–3474.
[18] J. Pérez-Ramírez, S. Abelló, N.M. van der Pers, Memory effect of activated Mg–Al hydrotalcite: *in-situ* XRD studies during decomposition and gas-phase reconstruction, Chem.: Eur. J., 13 (2007) 870–878.
[19] P. Cai, H. Zheng, C. Wang, H. Ma, J. Hu, Y. Pu, P. Liang, Competitive adsorption characteristics of fluoride and phosphate on calcined Mg–Al–CO$_3$ layered double hydroxides, J. Hazard. Mater., 213–214 (2012) 100–108.
[20] L. Ma, X. Zhang, D. Lin, Y. Chun, Q. Xu, Preparation of shaped magnesium oxide/carbon catalysts using rice grains as an exotemplate and carbon precursor, Appl. Catal., A, 460–461 (2013) 26–35.
[21] F. Jiao, J. Yu, H. Song, X. Jiang, H. Yang, S. Shi, X. Chen, W. Yang, Excellent adsorption of Acid Flavine 2G by MgAl-mixed metal oxides with magnetic iron oxide, Appl. Clay Sci., 101 (2014) 30–37.
[22] J.P. Nguetnkam, R. Kamga, F. Villiéras, G.E. Ekodeck, A. Razafitianamaharavo, J. Yvon, Alteration of cameroonian clays under acid treatment. Comparison with industrial adsorbents, Appl. Clay Sci., 52 (2011) 122–132.
[23] B. Cheng, Y. Le, W. Cai, J. Yu, Synthesis of hierarchical Ni(OH)$_2$ and NiO nanosheets and their adsorption kinetics and isotherms to Congo red in water, J. Hazard. Mater., 185 (2011) 889–897.
[24] M. Doğan, H. Abak, M. Alkan, Adsorption of methylene blue onto hazelnut shell: kinetics, mechanism and activation parameters, J. Hazard. Mater., 164 (2009) 172–181.
[25] R. Li, J.J. Wang, B. Zhou, M.K. Awasthi, A. Ali, Z. Zhang, L.A. Gaston, A.H. Lahori, A. Mahar, Enhancing phosphate adsorption by Mg/Al layered double hydroxide functionalized biochar with different Mg/Al ratios, Sci. Total Environ., 559 (2016) 121–129.
[26] Q. Sun, B. Chen, Biotemplated fabrication of 3D hierarchically porous MgAl-LDH/CF composites with effective adsorption of organic dyes from wastewater, Ind. Eng. Chem. Res., 59 (2020) 16838–16850.

[27] S.S. Baral, S.N. Das, P. Rath, Hexavalent chromium removal from aqueous solution by adsorption on treated sawdust, Biochem. Eng. J., 31 (2006) 216–222.

[28] N. Beigi, H. Shayesteh, S. Javanshir, M. Hosseinzadeh, Pyrolyzed magnetic NiO/carbon-derived nanocomposite from a hierarchical nickel-based metal-organic framework with ultrahigh adsorption capacity, Environ. Res., 231 (2023) 116146, doi: 10.1016/j.envres.2023.116146.

[29] S. Vreysen, A. Maes, Adsorption mechanism of humic and fulvic acid onto Mg/Al layered double hydroxides, Appl. Clay Sci., 38 (2008) 237–249.

[30] C.-Y. Kuo, C.-H. Wu, J.-Y. Wu, Adsorption of direct dyes from aqueous solutions by carbon nanotubes: determination of equilibrium, kinetics and thermodynamics parameters, J. Colloid Interface Sci., 327 (2008) 308–315.

[31] L. Zhang, P. Hu, J. Wang, Q. Liu, R. Huang, Adsorption of methyl orange (MO) by Zr(IV)-immobilized cross-linked chitosan/bentonite composite, Int. J. Biol. Macromol., 81 (2015) 818–827.

[32] M. Stoller, J.M.O. Pulido, L. di Palma, A.M. Ferez, Membrane process enhancement of 2-phase and 3-phase olive mill wastewater treatment plants by photocatalysis with magnetic-core titanium dioxide nanoparticles, J. Ind. Eng. Chem., 30 (2015) 147–152.

[33] S. Keleşoğlu, M. Kes, L. Sütçü, H. Polat, Adsorption of methylene blue from aqueous solution on high lime fly ash: kinetic, equilibrium, and thermodynamic studies, J. Dispersion Sci. Technol., 33 (2012) 15–23.

[34] R.-r. Shan, L.-g. Yan, K. Yang, S.-j. Yu, Y.-f. Hao, H.-q. Yu, B. Du, Magnetic Fe_3O_4/MgAl-LDH composite for effective removal of three red dyes from aqueous solution, Chem. Eng. J., 252 (2014) 38–46.

[35] A.M.M. Vargas, A.L. Cazetta, M.H. Kunita, T.L. Silva, V.C. Almeida, Adsorption of methylene blue on activated carbon produced from flamboyant pods (*Delonix regia*): study of adsorption isotherms and kinetic models, Chem. Eng. J., 168 (2011) 722–730.

[36] Y. Ding, L. Liu, Y. Fang, X. Zhang, M. Lyu, S. Wang, The adsorption of dextranase onto Mg/Fe-layered double hydroxide: insight into the immobilization, Nanomaterials, 8 (2018) 173, doi: 10.3390/nano8030173.